IN-48
026098

Wavelet Analysis of SAR Images for Coastal Monitoring

Antony K. Liu, Sunny Y. Wu

Oceans and Ice Branch, NASA Goddard Space Flight Center

Greenbelt, MD 20771, U.S.A.

and William Y. Tseng, William G. Pichel

Ocean Research and Application Division, NOAA/NESDIS

Washington, DC 20233, U.S.A.

Submitted to the Canadian Journal of Remote Sensing for ADRO Special Issue

Abstract

The mapping of mesoscale ocean features in the coastal zone is a major potential application for satellite data. The evolution of mesoscale features such as oil slicks, fronts, eddies, and ice edge can be tracked by the wavelet analysis using satellite data from repeating paths. The wavelet transform has been applied to satellite images, such as those from Synthetic Aperture Radar (SAR), Advanced Very High-Resolution Radiometer (AVHRR), and ocean color sensor for feature extraction. In this paper, algorithms and techniques for automated detection and tracking of mesoscale features from satellite SAR imagery employing wavelet analysis have been developed. Case studies on two major coastal oil spills have been investigated using wavelet analysis for tracking along the coast of Uruguay (February 1997), and near Point Barrow, Alaska (November 1997). Comparison of SAR images with SeaWiFS (Sea-viewing Wide Field-of-view Sensor) data for coccolithophore bloom in the East Bering Sea during the fall of 1997 shows a good match on bloom boundary. This paper demonstrates that this technique is a useful and promising tool for monitoring of coastal waters.

Notation

a : length scale of wavelet transform

$\underline{b}$: shift vector of wavelet transform

$g(x, y)$: Gaussian function

x : horizontal spatial coordinate

y : vertical spatial coordinate

T : value of threshold

$W_s(a, \underline{b})$: wavelet transform

Introduction

Satellite remote sensing technology can provide sea surface data with far better spatial and temporal coverage than that of the conventional *in-situ* measurements. With the aid of the satellite remote sensing imagery, it is now possible to monitor the ocean, particularly coastal water, with adequate temporal and spatial coverage for marine pollution and biological productivity. Sequential satellite images obtained from the AVHRR and SeaWiFS can be used to track mesoscale oceanic features. However, AVHRR and SeaWiFS images are obscured by cloud cover and low light levels limiting their usefulness. The advent of RADARSAT with ScanSAR of 500 km swath, can cover most of coastal areas in three days which is a powerful tool for coastal monitoring. Furthermore, using SAR in conjunction with AVHRR and SeaWiFS, the mesoscale features can be identified as caused by physical, biologocal, or sea surface temperature processes.

The two dimensional wavelet transform is a very efficient bandpass filter, which can be used to separate various scales of processes and show their relative phase/location (Combes et al., 1989). The two-dimensional Gaussian wavelet (often referred to as a "Mexican hat" wavelet) has been applied to satellite images to separate various scale processes including relative phase/location information for coastal applications (Liu, et al., 1997a) and for ice edge and ice floe tracking (Liu, et al., 1997b). The wavelet

transforms of SAR images can be used for near real-time "quick look" screening of satellite data (feature detection), data reduction (binary image), and image enhancement (edge linking). Wavelet analysis of SSM/I (Special Sensor Microwave/Imager) radiance data and NSCAT (NASA Scatterometer) backscatter data has been developed to obtain daily sea-ice drift information for both the northern and southern polar regions (Liu and Cavalieri, 1998; Liu et al., 1998).

In this paper, case studies on two major coastal oil spills is presented, which have been captured by the SAR and the AVHRR sensors on board of several satellites. The detection and tracking of the oil slicks are achieved by means of two-dimensional Gaussian-based wavelet analysis. The coccolithophore bloom in the East Bering Sea detected by SeaWIFS during the fall of 1997 has been studied by using SAR images to extract features near the bloom boundary.

Wavelet Analysis

Basically, wavelet transforms are analogous to Fourier transforms, but are localized both in frequency and time. The two-dimensional wavelet transform is a form of spatial differentiation. The resulting image is a differential image with accentuated amplitude changes. Furthermore, the Laplacian of Gaussian wavelet transform, one of the two employed in this analysis, works as a band-passed filter. Ideally only features with length scale within a chosen band are retained upon transformation.

The wavelet transform, $W_s(a,\underline{b})$, of a function, $s(\underline{r})$, where $\underline{r} = (x,y)$, is expressed in terms of the complex valued wavelet function, $w(\underline{r})$, as follows:

$$W_s(a,\underline{b}) = \frac{1}{\sqrt{a}} \int s(\underline{r}) w^*(\frac{\underline{r} - \underline{b}}{a}) d\underline{r} \quad \ldots\ldots\ldots\ldots\ldots (1)$$

in which the wavelet function is dilated by a factor a, and shifted by $\underline{b}$. The function $w(\underline{r})$ is the basic wavelet which must satisfy the admissibility condition, but is otherwise subject to choice within certain limits. Thus, the continuous wavelet transform ensures global energy conservation. The superscript (*) indicates complex conjugate. For data analysis, the mother wavelets frequently used are: a Gaussian-modulated sine and cosine wave packet (the Morlet wavelet); or the second derivative of a Gaussian function (the Mexican hat). In this study, the analyzing wavelet (a real value function) is defined as the second derivative of a Gaussian function centered about the origin. The equation for the Gaussian is given as:

$$g(x,y) = -a \exp(-\frac{x^2 + y^2}{2a^2}) \quad \ldots\ldots\ldots\ldots (2)$$

where a is the scale of the wavelet transform. Since convolution is commutative with respect to differentiation, the resulting wavelet transform is the Laplacian of a Gaussian smoothed function. Thus, its zeroes correspond to the inflection points of the original function. The contours of zero crossing indicate the edges in the pattern of the input function. The wavelet transform is calculated as a convolution in the fast Fourier

transform (FFT) domain and has computational efficiency. The Mexican hat wavelet has a close form, so it can be used directly for operation without recursive scheme to generate the wavelet base function.

To perform the wavelet transformation, first a suitable a value is chosen, which corresponds to the length scale of the Gaussian function. The general rule of thumb is to choose this value based on 1) the length scale of the feature of interest; and 2) the resolution (or pixel spacing) of the original image. A differential detection is then carried out to determine the pixel locations of significant differentials so that the feature of interest can be delineated from the background. In this paper, both kinds of wavelet-transformed data ($w1$, the first derivative and $w2$, the second derivative) are examined. An edge is expected to locate at pixel (x_0, y_0) if both of the following conditions are met:

$w1(x_0, y_0)$ exceeds a chosen threshold value T, where $T = \overline{[w1(x,y)]} + t \times [w1(x,y)]'$, and

$\overline{[w]}$: the ensemble average;

$[w]'$: the standard deviation of the ensemble.

$w2(x_0, y_0)$ equals to a predetermined value c which is typically in the neighborhood of zero.

The choices of t and c rely to a great extent on the observation as to where the actual edges lie, which can be achieved by visual inspection. For noise-free images, the threshold t can be chosen such that all amplitude changes above a minimum contrast level are detected as edges, and all others are considered non-edges. With noisy images, such as

SAR with speckle noise, the threshold selection becomes a tradeoff between missing valid edges and designating noise-induced false edges.

The Laplacian $G(x,y)$ of the original image $F(x,y)$ is zero if $F(x,y)$ is constant or changing linearly in amplitude. If the rate of change of $F(x,y)$ is greater than linear, $G(x,y)$exhibits a sign change at the point of inflection of $F(x,y)$. The zero crossing of $G(x,y)$ thus indicates the presence of an edge. In reality, since SAR imagery is subject to heavy "speckle noises", the rate of the change of the original image ($F(x,y)$) equals to zero at many pixel locations throughout the image. The zero crossings of $G(x,y)$ under this circumstance are clearly false edges. Therefore, it often becomes necessary to find a suitable value other than zero for c. By properly selecting a non-zero contour value, Liu *et. al.* (1997a) has shown that one can pick out the valid edges while reducing the amount of the false edges by as much as 80%. Obviously, in order to keep the edges identified in a sufficiently narrow band of the point of the inflection of $F(x,y)$, the contour value has to be sufficiently close to zero.

Case Study of Oil Spills in Uruguay

On February 8, 1997, a major oil spill occurred at the mouth of Rio de la Plata River between Uruguay and Argentina. The leakage was from a passing oil tank. In response to this incident, NESDIS has acquired several images of the area taken a few days afterwards by SAR on board the Canadian RADARSAT and by AVHRR on board a

NOAA satellite. The procedure to collect SAR data is not designed for real-time response of a sudden incident and the SAR image is finally collected over this area on February 26, 1997. After examining all AVHRR images covered in this period, only two AVHRR images among them have clearly captured the spreading of the initial oil spill in sequence. Before being subjected to wavelet analysis, some imagery may require preprocessing using conventional image processing techniques. The preprocessing of SAR image from the RADARSAT is described as follows.

Collected on February 26, 18 days after the onset of the oil spill, the original ScanSAR image from the RADARSAT has a dimension of 12592*18392 pixels with 25 m pixel spacing. A subscene of 1024*1024 pixels showing the spread of oil slicks was cropped out from a smoothed (8*8 pixel-averaged) ScanSAR image. The gray-scale histogram of this subscene (Figure 1) shows distinct two and a half peaks. One of them is centered on high gray-scale (90) and consists of the pixels on land and in clear water. The other one is centered on medium gray-scale (50) and consists of the pixels in the oil-contaminated water. The half peak at lowest gray-scale (0) consists of pixels in the contaminated area covered with the thickest oil film. In order to sufficiently separate the three distinctive surfaces, the technique of linear stretch of gray-level values is used to enhance the contrast between features represented by any two adjacent peaks in the histogram. The wavelet transform technique is then applied separately to the two contrast-enhanced images: one stressing contrast between land/clear water and oil-contaminated water, and the other stressing contrast between the less contaminated water and the more contaminated one.

For RADARSAT SAR image collected on February 26, 1997, several different a values (2^2, 2^3, 2^4) have been tested in this study. It was found that the wavelet transform with a = 8 best matches the oil slicks in this case. In terms of the real dimension, this value corresponds to a length scale of L = 8 * 200 m = 1.6 km. By combining the edges detected from the two contrast-enhanced images separately, we obtain a clear picture as to where the oil slicks have spread to and where the thicker oil films was located (Figure 2).

Many images taken by the AVHRR sensor on board a NOAA satellite a few days earlier than the RADARSAT flight are also acquired and examined in this study. The AVHRR sensor measures emitted and reflected radiance in four or five spectral bands, spanning from visible portion of the spectrum to the thermal infrared. Only two images (each with ~1 km pixel spacing), from band 1 (a visible band, taken on February 13, 1997) and band 4 (infrared, taken on February 15, 1997), have best captured the signature of the oil spill and have therefore been chosen to be studied using wavelet analysis. Two subscenes of 256×256 pixels were cropped out from the original AVHRR images, both having a dimension of 490×403 pixels. To delineate the oil spill, the a values for both images were chosen to be 4, corresponding to a length scale of L = 4 * 1 km = 4 km. The threshold values t for bands 1 and 4 are 0.1 and 0.2, respectively. Figures 3 and 4 show the results of the wavelet analysis of these two AVHRR images from February 13 and 15, 1997 respectively. From the tracking results of wavelet analysis, it is clearly that the oil films had been drifting downstream mainly along the Uruguay coast. The spreading pattern suggests that the dispersion played a key role for a period of time at first, then wind and

wind-induced current took over the process. By February 26, two and a half weeks after the incident, the spill has been broken into smaller patches of slick and spread out all over the coast along Uruguay. But, a distinct boundary of oil contaminated region along the coast is still well observable and can be clearly identified in the results. Based on band 1 AVHRR image from February 15, the sediment from the river was drifting southward along the Argentina coast. Therefore, the spread of oil spill is most likely forced by wind not by current from the river.

Oil Spills near Point Barrow, Alaska

In early November 1997, shortly after the satellite RADARSAT had resumed its coverage of the Arctic region, the SAR sensor on board captured an oil spill off Point Barrow, Alaska. The oil slicks show up clearly on the RADARSAT ScanSAR imagery on November 2, 3 and 9. The oil spill is suspected to be related with the Alaskan Oil Pipeline, although the exact source remains unknown. Three subscenes of 1024 * 1024 pixels with 100 m resolution containing the oil slicks was cropped out from each of the original ScanSAR images for analysis.

Among the three SAR images, the oil slicks on November 2 have the most well-defined shape, apparently as the result of the low wind and calm sea. The matching a value for the wavelet analysis is 8, corresponding to a length scale of L = 8 * 100 m = 800 m. The threshold t is chosen to be 0.6. Figure 5 shows the result of wavelet analysis with the oil

slicks delineated. The oil spills are separated by three patches and lined up in the north-south direction.

On November 3, the wind had obviously become stronger with wind streaks as shown in Figure 6. The wind streaks from the SAR image follow the northwest or southeast direction. The oil slicks had broken into a series of elongated patches. A much smaller a = 2 is used in order to delineate them. This value corresponds to a length scale of L = 2 * 100 m = 200 m. The threshold is chosen to be 2.4. In general, as a becomes smaller, the differential detection picks up more fine details. The threshold t is then raised to offset the effect. The shapes of oil slick patches are not well-defined due to the strong wind drift. Therefore, the outlines of some of the less distinguishable oil slicks are missed out as a consequence (Figure 6).

Six days later on November 9, the oil slicks had drifted further offshore toward northwest and become two elongate patches. Figure 7 shows a subscene from the SAR image collected on November 9 with the oil slicks delineated by wavelet transform. The relevant parameters for the wavelet analysis are: a = 4 for wavelet length scale, and the threshold t = 2.2. Figure 8 shows a map of Point Barrow and its vicinity to summarize the approximate locations of the oil slicks and their tracks as they were drifted further offshore due to coastal wind.

Coccolithophore Bloom in the East Bering Sea

Coccolithophore bloom in the East Bering Sea was observed from NOAA's R.V. Miller Freeman in July, 1997 as an extraordinary warm water mass of intense aqua color. On July 29, 1997 the edge of aqua water is characterized by interleaf of aqua and darker bands of fingers. Recent composite SeaWiFS image (September 18 to October 3) show anomalous condition in the Bering Sea. ASF (Alaska SAR Facility) has collected ERS-2 quick-look SAR image on September 11, 1997 in the east Bering Sea. In this scene, there are many ships and appear to have some large wave patterns from the southwest corner of the scene, expanding towards the east. A RADARSAT ScanSAR image collected on September 6, 1997 shows many dark stripes in the Southeast Bering Sea, which may be related to the bloom. These dark stripes maybe the surface films drifted from the bloom area by strong northwestern wind.

A SeaWiFS pigment concentration image of Global Level data (4 km resolution) in the east Bering Sea on September 20, 1997 is shown in Figure 9. The western boundary of high pigment concentration area is indicated by a white arrow at 57.8 degree of Latitude and 172.0 degree of Longitude. On Sept. 20, the ERS-2 SAR image collected shows a clear frontal boundary right at the bloom edge (Figure 10). The boundary has been delineated by using wavelet transform with a scale $a = 32$ as an edge detector for large frontal boundary. The boundary is not perfectly delineated because of the edge effect from the SAR scene using large-scale wavelet transform. Multi-scale wavelet transform can be used to locate a more accurate boundary as demonstrated by Liu et al. (1997b). The dark circle with a cross is located at 58.1 degree of Latitude and 172.3 degree of

Longitude and matches well with the bloom boundary indicated in Figure 8 by arrow. The dark area inside the frontal boundary in SAR image is probably related to the surface film produced by coccolithophore bloom. Further inside the bloom area, even darker region can be clearly identified. Also, notice that many small circle features in this area are probably caused by rain cells. Since there were rain cells on both sides of frontal boundary, this is most likely not an atmospheric front but an oceanic front. Also, the sea surface temperature in this area is quite uniform and the temperture difference along can not induce such a large change of radar backscatter intensity across the boundary.

The reason why surface films are able to be detected on radar images is that oil films have a dampening effect on short surface waves. Radar is remarkably sensitive to small changes in the roughness of the sea. The dark appearance on radar images is due to the smooth ocean surface and is similar to the appearance of areas of low winds. It is the distinctive shape and sharp boundary of surface film which enables them to be identified with a high degree of confidence.

Conclusions

The NOAA (National Oceanic and Atmospheric Administration) CoastWatch provides near real-time mapped satellite and in-situ data and information for U.S. coastal waters suitable for hazard warning, ice and ocean monitoring, and environmental management. A development project is underway to add SAR data and products to the CoastWatch

product suite. The use of wavelet transform techniques for the automated analysis of SAR, AVHRR, and SeaWiFS images to detect ocean features has been demonstrated for CoastWatch applications.

Remote sensing with repeated coverage is the most efficient method to monitor and study marine productivity and pollution. The mapping of mesoscale ocean features in the coastal zone is a major potential application for satellite SAR data, especially for the ScanSAR on RADARSAT with 500 km swath. The use of SAR-derived observations to track eddies, surface temperature-related features, and river and estuarine plumes can aid in the management of fisheries. Especially in the Alaska coast area, uniform cold sea surface temperatures and cloud cover preclude AVHRR measurements of surface temperature features, and obscure ocean color observations.

The wavelet transforms of satellite images can be used for near real-time "quick look" screening of satellite data (feature detection), data reduction (binary image), and image enhancement (edge linking). By combining ocean color (SeaWiFS or OCTS), SAR (ERS-2 or RADARSAT), and infrared (AVHRR) images (wavelet- transformed binary images) using some data fusion techniques, mesoscale features of various physical processes such as oil spills, surface slicks, fronts, upwelling, and eddies can be detected and tracked in the coastal zone. Wavelet analysis can provide a more cost-effective monitoring program that would keep track of changes in important elements of the coastal watch system. In this study, we have demonstrated that the two-dimensional Gaussian-based wavelet analysis is a very useful tool for data fusion from multi-sensors, such as

SAR, AVHRR, and SeaWiFS.

Acknowledgements

The authors would like to thank Kevin Arrigo for providing the SeaWiFS image. They also wish to thank Canadian Space Agency (CSA) and Alaska SAR Facility for providing and processing RADARSAT SAR data. Copyright of all RADARSAT SAR images belongs to CSA. This work was supported by ADRO Program of the National Aeronautics and Space Administration, and Coastal Ocean Program of the National Oceanic and Atmospheric Administration.

References

Combes, J. M., A. Grossmann, and Ph. Tchamitchian. 1989. "Wavelet: Time Frequency Methods and Phase Space", *Proc. International Conference*, Marseille, France, Springer-Verlag, 331pp.

Liu, A. K., C. Y. Peng, and S. Y.-S. Chang. 1997a. "Wavelet Analysis of Satellite Images for Coastal Watch", *IEEE Journal of Oceanic Engineering*, Vol. 22, No. 1, pp. 9-17.

Liu, A. K., S. Martin, and R. Kwok. 1997b. "Tracking of Ice Edge and Ice Floes by Wavelet Analysis of SAR Images", *Journal of Atmospheric and Oceanic Technology*, Vol. 14, pp. 1187-1198.

Liu, A. K., and D. J. Cavalieri. 1998 "Sea-Ice Drift from Wavelet Analysis of DMSP SSM/I Data", *International Journal of Remote Sensing*, Vol. 19, No. 7, pp. 1415-1423.

Liu, A. K., Y. Zhao, and W. T. Liu. 1998. "Sea Ice Motion Derived from Satellite Agrees with Buoy Observations", *EOS, Transactions*, American Geophysical Union, Vol. 79, pp. 353 & 359.

Figure Captions

Figure 1. The gray-scale histogram of the RADARSAT SAR subscene (1024*1024 pixels) collected on February 26, 1997.

Figure 2. The RADARSAT SAR subscene collected on February 26, 1997 with Uruguay coastline and surface film patches delineated by wavelet transform.

Figure 3. The AVHRR subscene of the mouth of the Rio de la Plata River collected on February 13, 1997. The c-shaped patch at the center of subscene is the oil slick delineated by the wavelet transform.

Figure 4. The AVHRR subscene collected on February 15, 1997 with Uruguay and Argentina coastlines, along with the oil slick delineated by the wavelet transform.

Figure 5. A subscene from the RADARSAT ScanSAR image of Alaska coast near Point Barrow collected on November 2, 1997 with oil slicks delineated by wavelet transform.

Figure 6. A subscene from the RADARSAT ScanSAR image of Alaska coast near Point Barrow collected on November 3, 1997 with oil slicks delineated by wavelet transform.

Figure 7. A subscene from the RADARSAT ScanSAR image of Alaska coast near Point Barrow collected on November 9, 1997 with oil spills delineated by wavelet transform.

Figure 8. A map of Point Barrow, Alaska and its vicinity. The three solid circles indicate the approximate locations of oil slicks at the date labeled.

Figure 9. A SeaWiFS image collected on September 20, 1997 in the east Bering Sea showing coccolithophore bloom in bright color with high pigment concentration. The western bloom boundary is indicated by a white arrow.

Figure 10. An ERS-2 SAR scene of 100 km * 100 km collected on September 20, 1997 in the east Bering Sea with bloom boundary delineated by wavelet transform. The dark circle corresponds to and matches with the bloom boundary indicated in Figure 8.

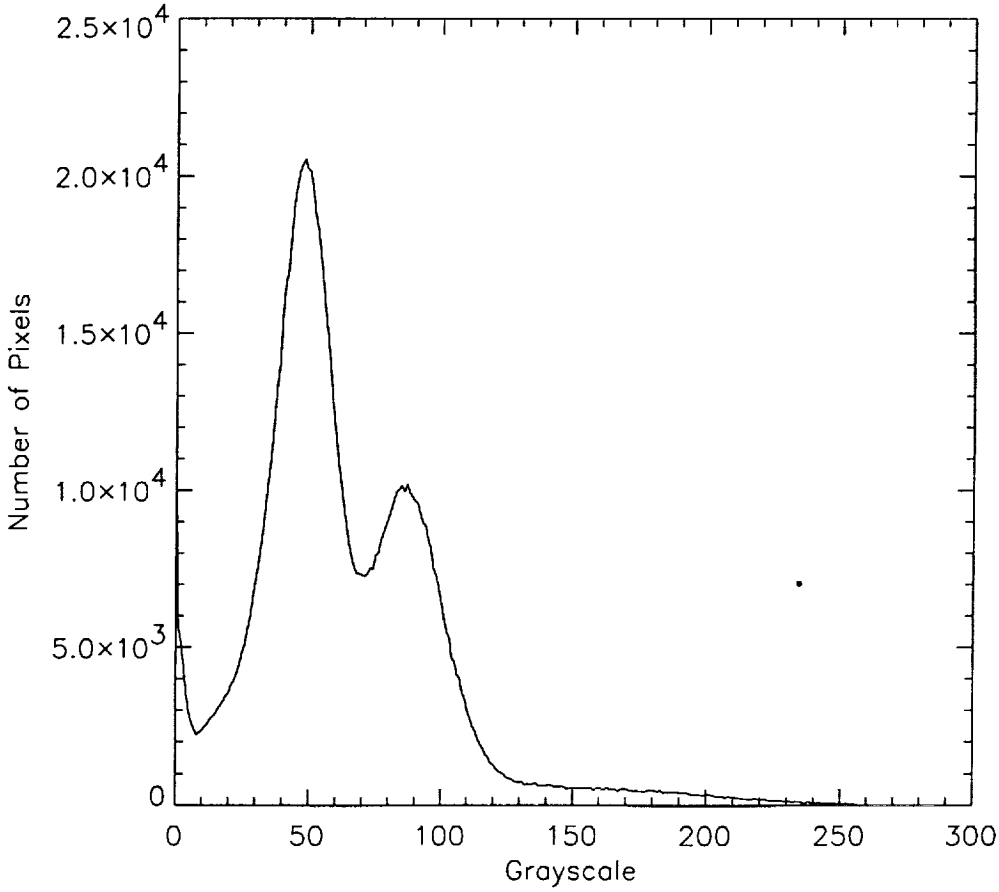
2.5×10^4
2.0×10^4
1.5×10^4
1.0×10^4
5.0×10^3
0
Number of Pixels
0
50
100
150
200
250
300
Grayscale

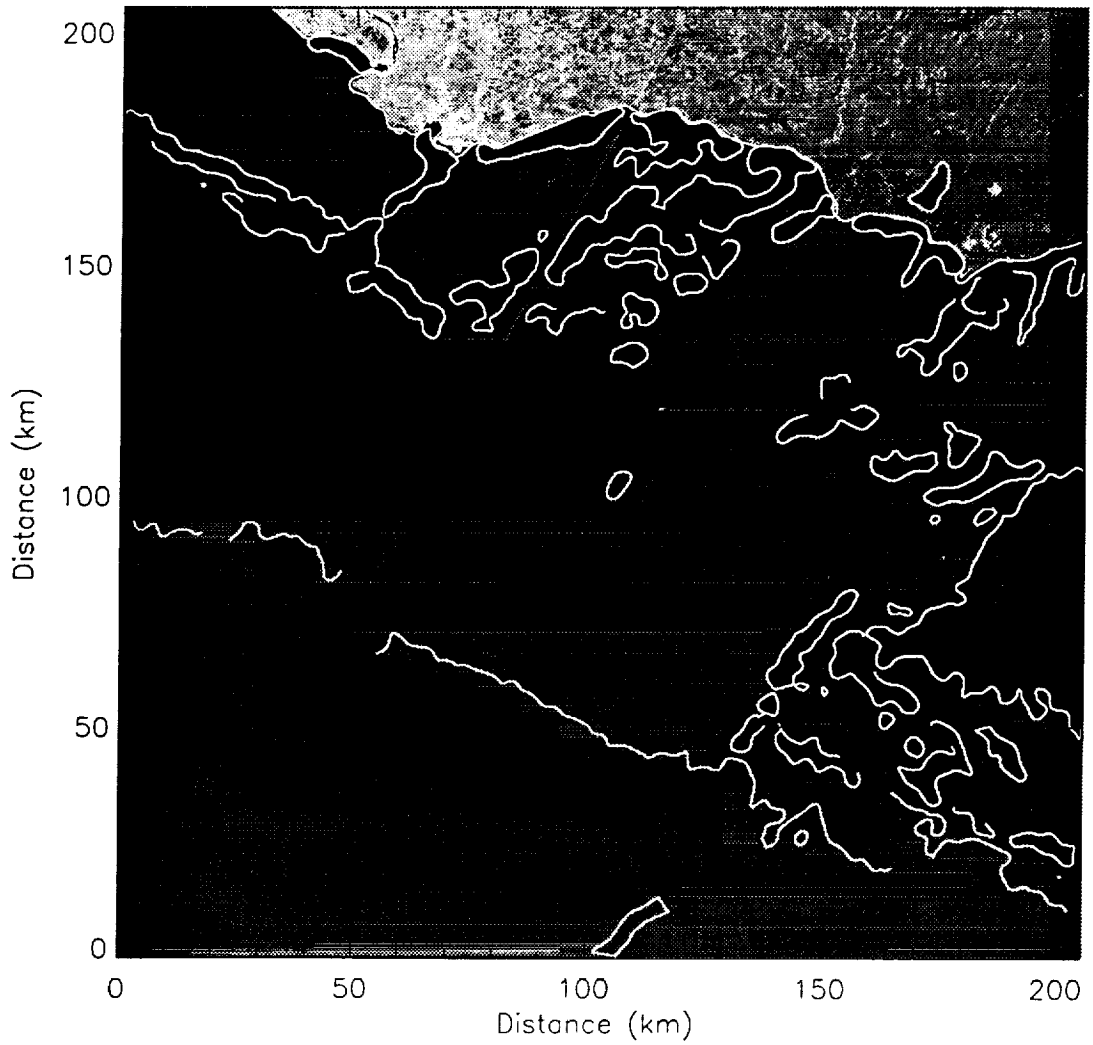
200
150
100
50
0
Distance (km)
0
50
100
150
200
Distance (km)

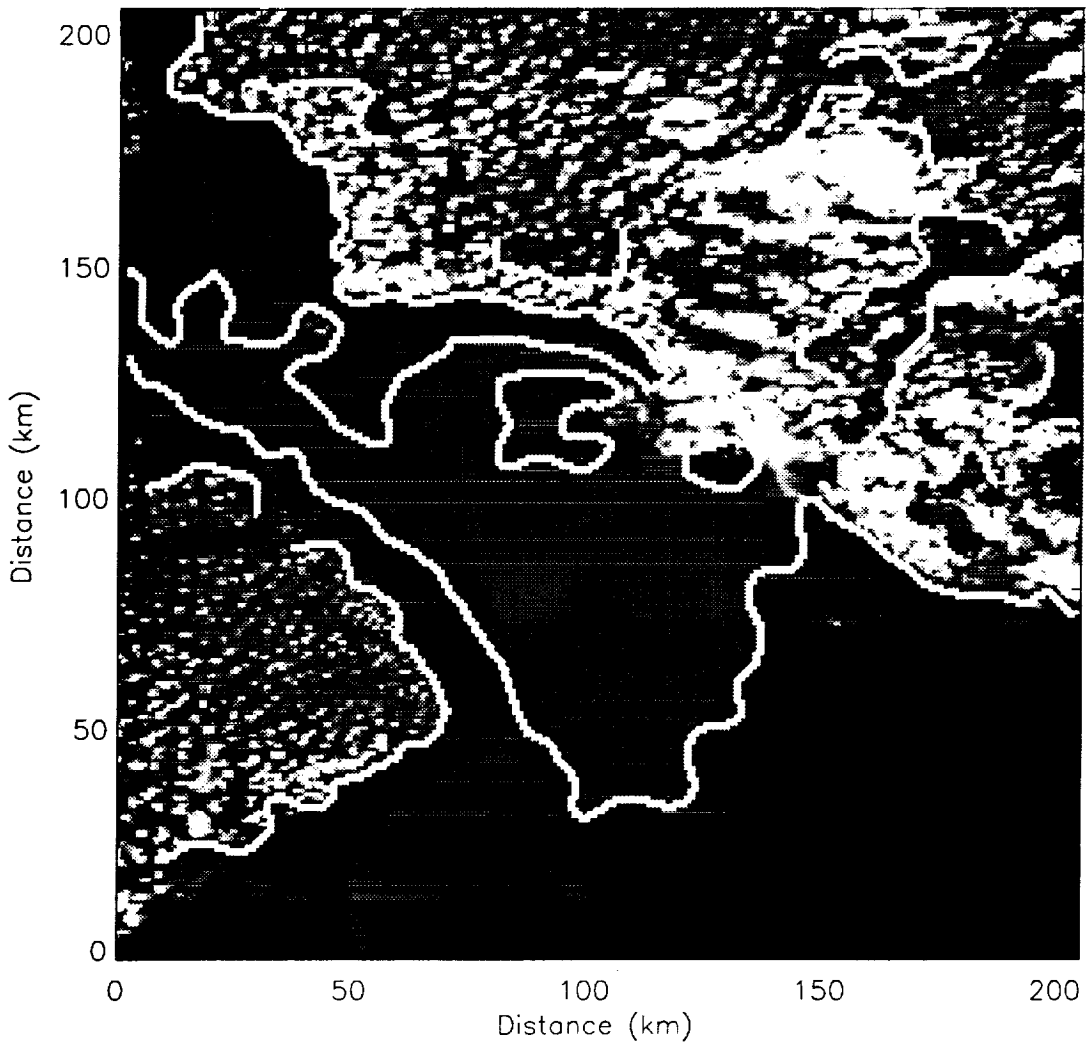
200
150
100
50
0
Distance (km)
0
50
100
150
200
Distance (km)

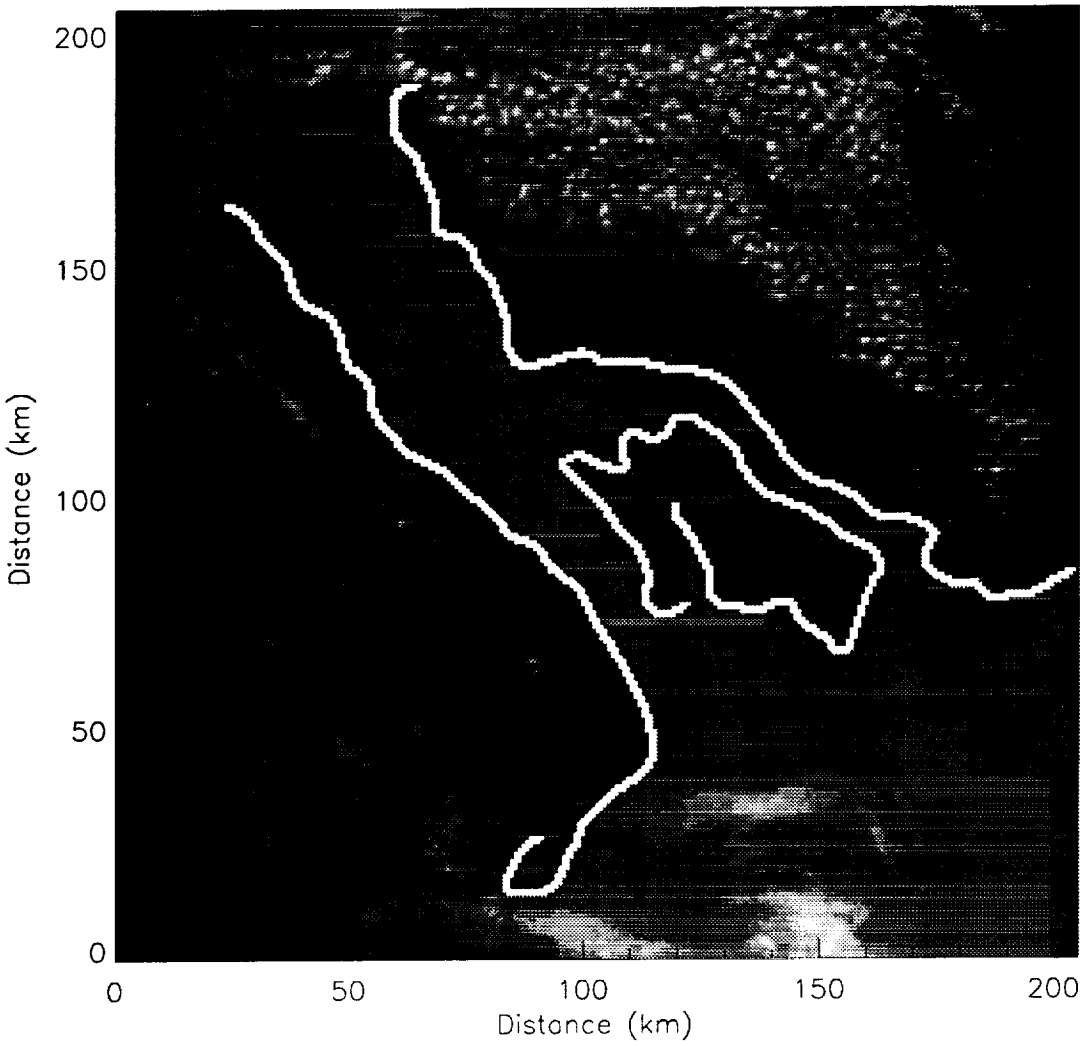
200
150
100
50
0
Distance (km)
0
50
100
150
200
Distance (km)

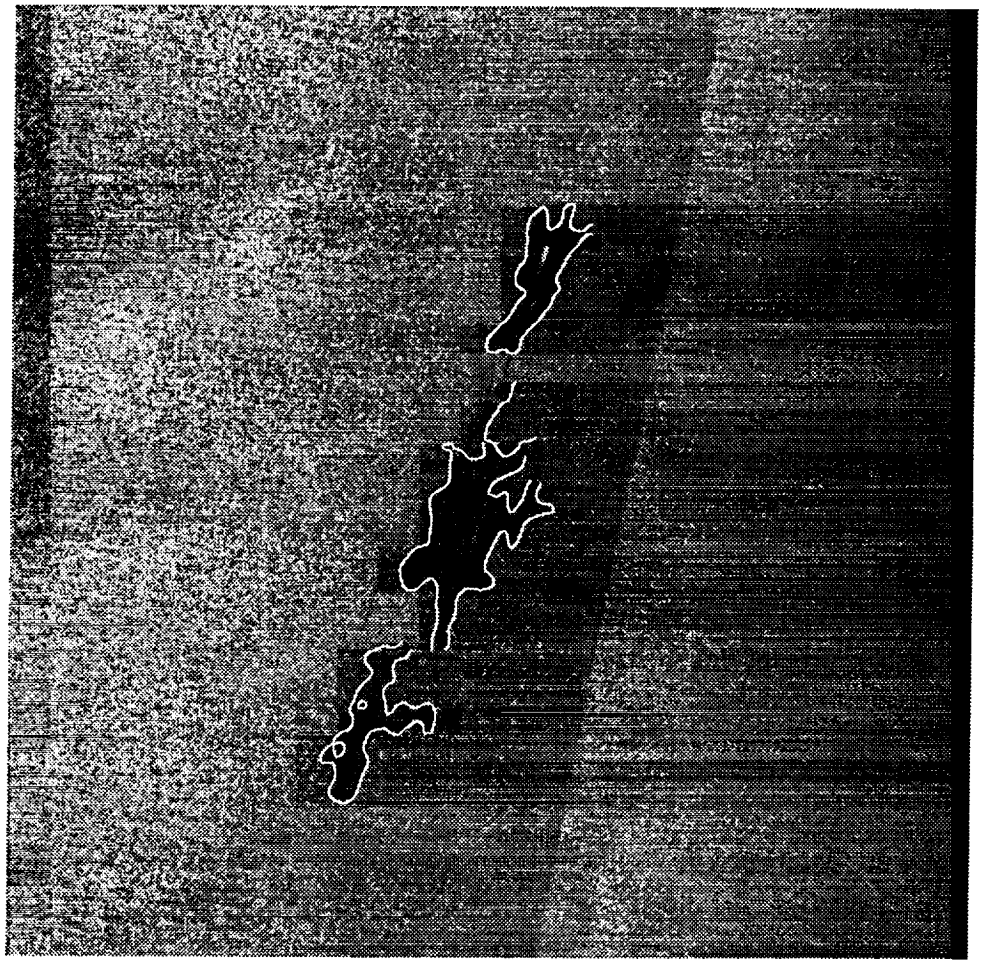

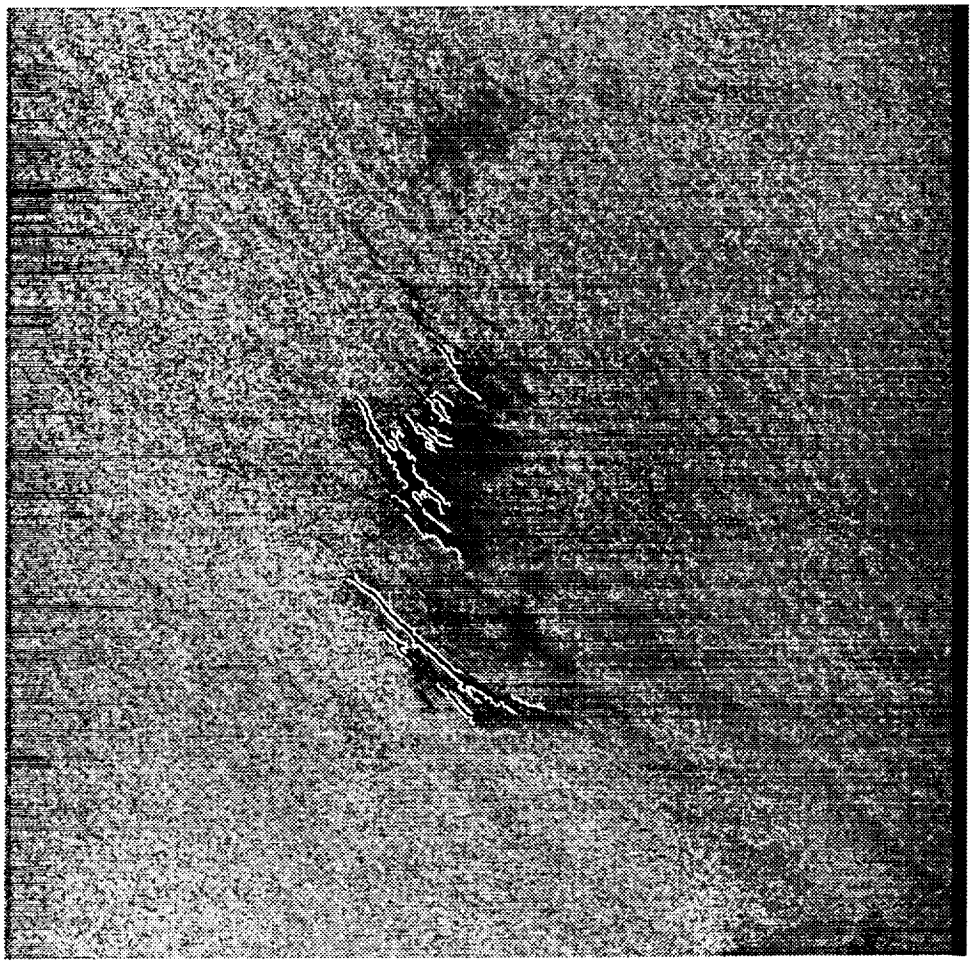

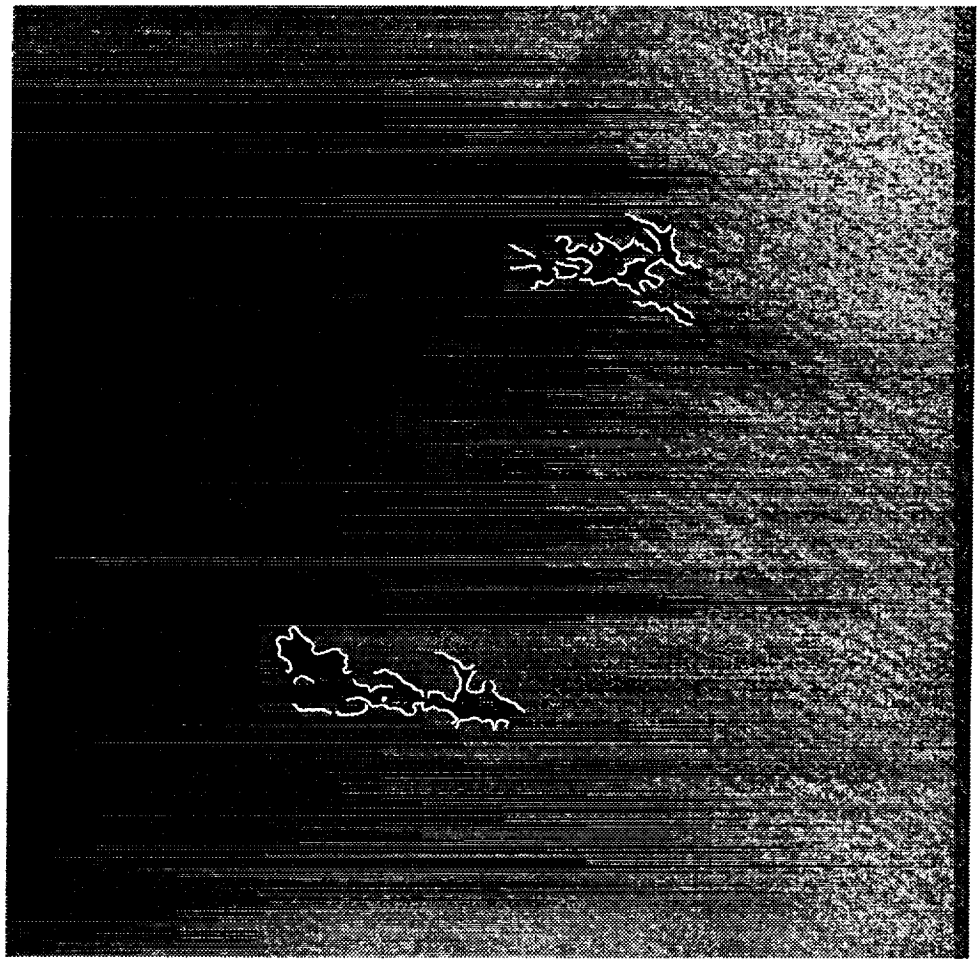

Location figure showing study area

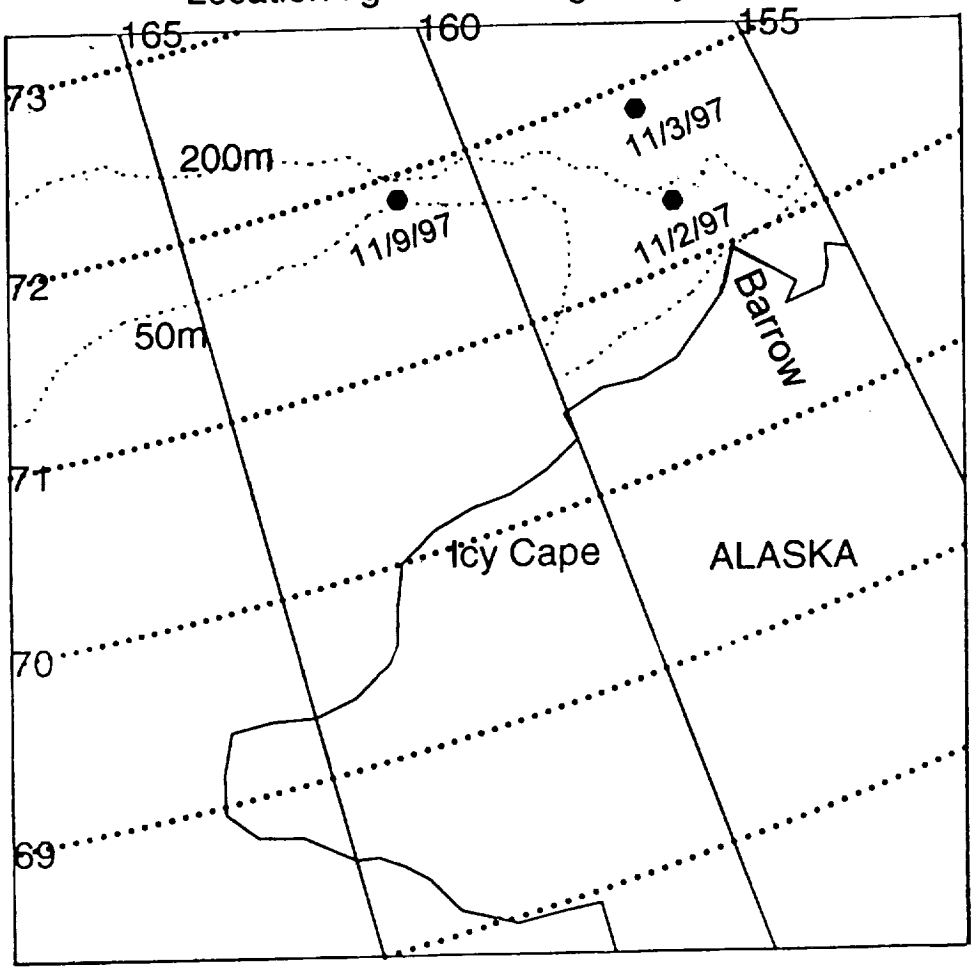

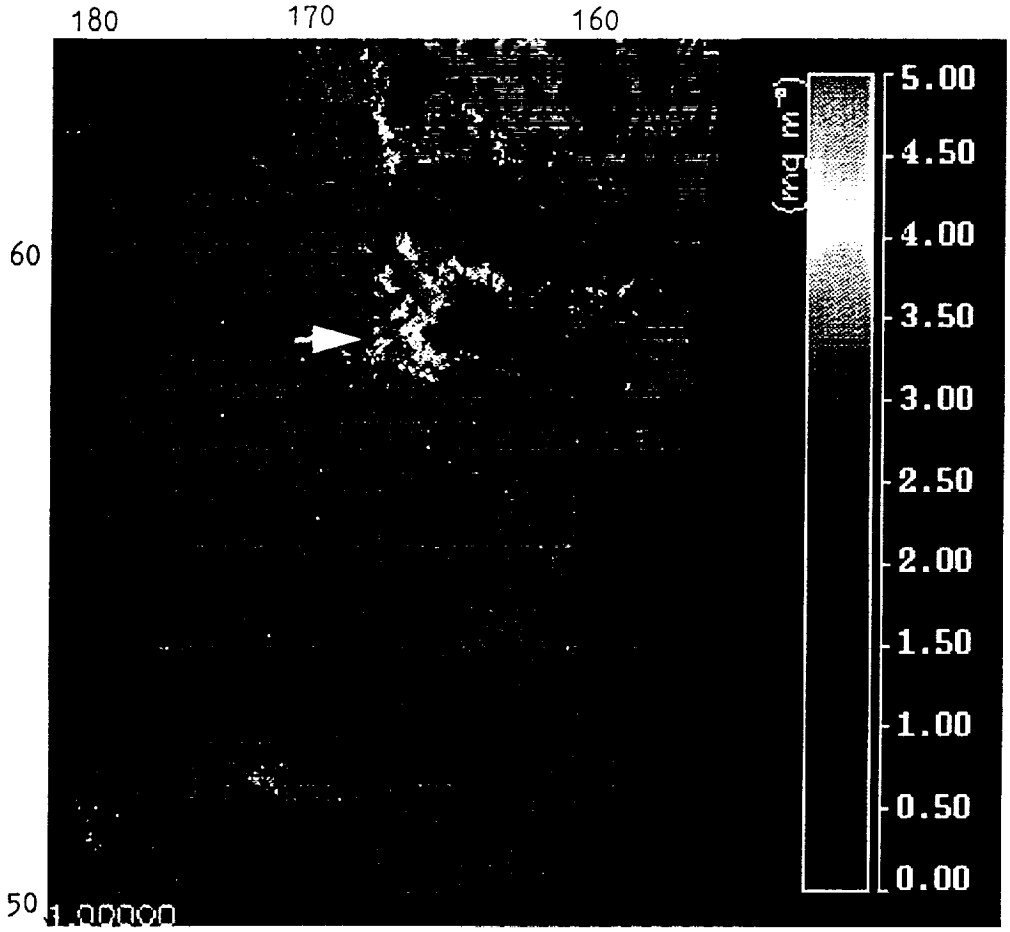
180
170
160
60
50
(mg m⁻³)
5.00
4.50
4.00
3.50
3.00
2.50
2.00
1.50
1.00
0.50
0.00

ERS2 SAR Image: Boundary of Coccolithophore Bloom in Bering Sea

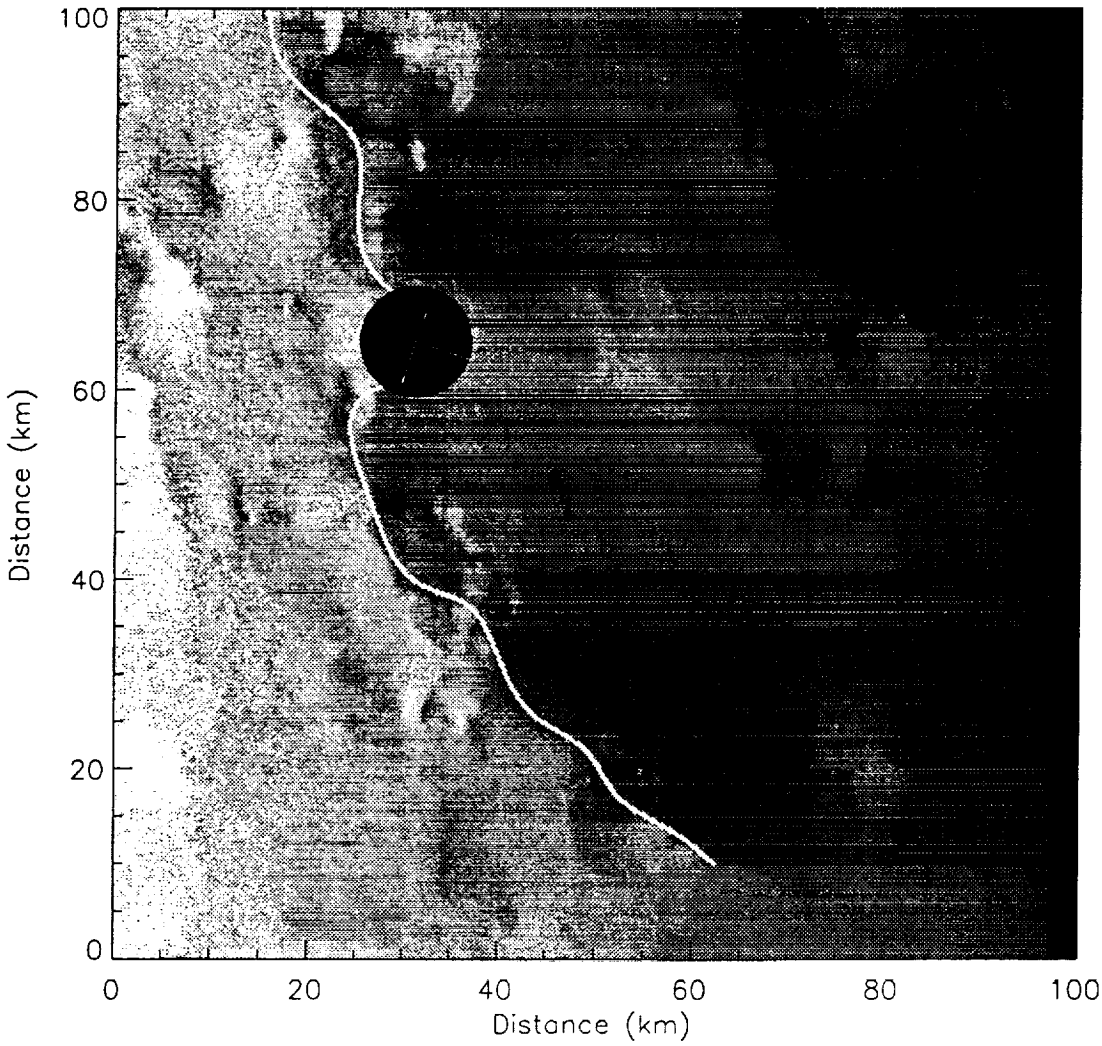

TITLE : Wavelet Analysis of SAR Images for Coastal Monitoring

AUTHORS: Antony K. Liu and Sunny Y. Wu, Oceans and Ice Branch, Code 971/GSFC
William Y. Tseng and William G. Pichel, Ocean Research and Application Division, NOAA/NESDIS

SIGNIFICANT FINDINGS:

Remote sensing with repeated coverage is the most efficient method to monitor and study marine productivity and pollution. The mapping of mesoscale ocean features in the coastal zone is a major potential application for satellite SAR data, especially for the ScanSAR on RADARSAT with 500 km swath. The wavelet transforms of satellite images can be used for near real-time "quick look" screening of satellite data (feature detection), data reduction (binary image), and image enhancement (edge linking). By combining ocean color (SeaWiFS or OCTS), SAR (ERS-2 or RADARSAT), and infrared (AVHRR) images (wavelet-transformed binary images) using some data fusion techniques, mesoscale features of various physical processes such as oil spills, surface slicks, fronts, upwelling, and eddies can be detected and tracked in the coastal zone. Wavelet analysis can provide a more cost-effective monitoring program that would keep track of changes in important elements of the coastal watch system. In this study, we have demonstrated that the two-dimensional Gaussian-based wavelet analysis is a very useful tool for data fusion from multi-sensors, such as SAR, AVHRR, and SeaWiFS.

TITLE : Wavelet Analysis of SAR Images for Coastal Monitoring

AUTHORS: Antony K. Liu and Sunny Y. Wu, Oceans and Ice Branch, Code 971/GSFC
William Y. Tseng and William G. Pichel, Ocean Research and Application Division, NOAA/NESDIS

RELATION TO MTPE STRATEGIC PLAN:
Research is directly related to the MTPE science goals relating to algorithm/ sensor development. This study provides new technique for satellite imaging processing and data products.